Materials Advances

ROYAL SOCIETY OF CHEMISTRY

PAPER

View Article Online
View Journal | View Issue

Cite this: *Mater. Adv.*, 2024, 5, 4764

A highly simple and controllable nitrogen-doping method for carbon-based surface-enhanced Raman spectroscopy substrates†

Machiko Marumi,[a] Xuke Tang,[a] V. Kesava Rao,[ab] Abdullah N. Alodhayb,[c] Manish M. Kulkarni,[d] Prabhat K. Dwivedi,[d] Fabio Lisi,[a] Yasutaka Kitahama,*[ab] Ting-Hui Xiao[aef] and Keisuke Goda*[abghi]

Surface-enhanced Raman spectroscopy (SERS) is a highly sensitive tool for label-free chemical analysis. Recently, carbon-based SERS substrates have gained preference over traditional metal-based ones because they possess uniform signal enhancement distribution, high biocompatibility, robust chemical stability, enhanced adsorption capacity, and high durability attributed to their reduced photothermal conversion. An important strategy for improving the SERS performance of carbon-based substrates is the incorporation of heteroatoms, particularly nitrogen (N). However, traditional N-doping methods are often complex and difficult to control. To address this challenge, we developed a simple and controllable N-doping method for preparing carbon-based SERS substrates. This method specifically manipulates N doping and expands the conjugated π-electron system in polyacrylonitrile (PAN)-based substrates by adjusting the pyrolysis temperature (up to 1200 °C) within a low vacuum environment (0.2 Pa) over a brief period (2 min). Interestingly, our PAN-based substrates, enriched with N atoms, demonstrated 7.5–20 times stronger Raman signal enhancement than graphite substrates commonly used in SERS experiments. This innovative fabrication method is expected to broaden the practical use of SERS substrates in various sensing applications.

Received 4th February 2024,
Accepted 19th April 2024

DOI: 10.1039/d4ma00113c

rsc.li/materials-advances

1. Introduction

Surface-enhanced Raman spectroscopy (SERS) is a highly sensitive tool for multiplexed and label-free detection.[1–6] While traditional SERS substrates primarily consist of metal-based materials, distinguished by significant enhancement factors (EFs) and devoid of inherent SERS signals,[1–13] there has been a substantial shift toward exploring efficient metal-free alternatives, particularly those made from carbon-based materials.[14–38] Such metal-free substrates enhance the Raman signal by forming a charge-transfer (CT) complex between the analyte and the substrate. This interaction modifies the electronic energy levels and amplifies the Raman signal *via* the resonance Raman effect, a process known as the "chemical enhancement mechanism". This mechanism differs distinctly from the electromagnetic process prevalent in metallic substrates, which depends on surface plasmon resonance (SPR).[1–6] Compared to metallic substrates, metal-free substrates offer numerous benefits. They provide a more uniform signal enhancement distribution and possess enhanced durability because of reduced photothermal conversion *via* plasmon-free signal enhancement.[22–34] These attributes make metal-free substrates an increasingly attractive choice for a wide range of applications in SERS.

Among metal-free substrates, carbon-based ones are highly favored for plasmon-free SERS in the visible region SPR due to their high chemical stability, biocompatibility, and adsorption capacity.[36] The efficiency of SERS is notably enhanced by the π–π stacking of sp^2 domains, which has led to the popularity of materials such as graphene, graphite, and amorphous carbon

[a] *Department of Chemistry, The University of Tokyo, Tokyo 113-0033, Japan. E-mail: kitahama@g.ecc.u-tokyo.ac.jp, goda@chem.s.u-tokyo.ac.jp*
[b] *LucasLand, Tokyo 101-0052, Japan*
[c] *Department of Physics and Astronomy, College of Science, King Saud University, Riyadh, 11451, Saudi Arabia*
[d] *Centre for Nanosciences, Indian Institute of Technology Kanpur, Kanpur 208016, India*
[e] *Henan Key Laboratory of Diamond Optoelectronic Materials and Devices, School of Physics and Microelectronics, Zhengzhou University, Zhengzhou 450052, China*
[f] *Institute of Quantum Materials and Physics, Henan Academy of Sciences, Zhengzhou 450046, China*
[g] *Institute for Quantum Life Science, National Institute for Quantum and Radiological Science and Technology, Chiba 263-8555, Japan*
[h] *Institute of Technological Sciences, Wuhan University, Hubei 430072, China*
[i] *Department of Bioengineering, University of California, Los Angeles, California 90095, USA*

† Electronic supplementary information (ESI) available. See DOI: https://doi.org/10.1039/d4ma00113c

as SERS substrates. Notably, doping these materials with heteroatoms, particularly nitrogen (N), has been widely explored to improve SERS performance even further. N doping positively impacts the energy levels, often shifting the Fermi level and occasionally increasing the bandgap energy,[37,38] thereby enhancing the SERS efficiency.

Traditionally, N doping has been achieved through complex methods such as solvothermal synthesis under high pressure and temperature in autoclaves[29,30] or ionization with ultrashort femtosecond pulsed lasers.[31] An alternative approach involves the pyrolysis of N-containing precursors such as poly(4-vinylpyridine) and polydopamine.[32–34] However, these techniques often result in inevitable incomplete carbonization, leading to smaller conjugated π-electron systems and diminished enhancement effects. Balancing these competing processes and achieving control over them remain considerable challenges, highlighting the need for new fabrication methods for yielding highly efficient carbon-based SERS substrates.

To address this, we introduce a simple and controllable N-doping method using the carbonization of electrospun polyacrylonitrile (PAN) nanomesh for preparing carbon-based SERS substrates. Although the carbonization of PAN has been well documented,[39–41] where polymer chains transition to a ladder structure at temperatures above 250 °C, N is eliminated above 600 °C, and the graphite structure is eventually adopted near 3000 °C without requiring a metal catalyst,[42,43] its impact on SERS performance has not been previously explored. To fill this gap, we conducted a systematic examination of the chemical and structural transformations of PAN nanomesh carbonized at different temperatures. The results obtained were then used to theoretically elucidate alterations in the chemical enhancement observed in SERS. The PAN-based substrates exhibited SERS EFs of 6800 and 3200 for rhodamine 6G (R6G) and crystal violet (CV), respectively. These values exceed those obtained with conventional graphite substrates in SERS by approximately 30-fold. Crucially, this investigation led to the development of a simple and controllable method for preparing N-doped carbon-based SERS substrates, marking a considerable advancement in the field of metal-free SERS.

2. Methods

2.1. Materials

PAN and R6G were purchased from Sigma Aldrich. Dimethyl sulfoxide (DMSO) and CV were purchased from FUJIFILM Wako Pure Chemical Corporation. All chemicals were used without further purification. Silicon (Si) wafers and graphite sheets were purchased from AS ONE and PERMA-FOIL(R), respectively.

2.2. Characterization

Scanning electron microscopy (SEM, JSM-6610LV) was used to observe morphological structures, using a field-emission energy source of 5 kV. Infrared absorption (IR) spectroscopy (Shimadzu Trace-100 FT-IR spectrometer) was used to explore the functional groups in the PAN-based SERS substrates. The bulk chemical composition was examined using energy-dispersive X-ray spectroscopy (EDS, Aztec Energy). X-ray photoelectron spectroscopy (XPS, PHI5000 VersaProbe) was employed to investigate the chemical bonds on the surface of the sample, using a standard X-ray source, Al Kα radiation (1486.6 eV), and maximizing the focus size. Spontaneous Raman spectroscopy with a 532-nm excitation laser was used to evaluate the degree of carbonization in the PAN-based SERS substrates. CT between the PAN-based SERS substrate and the analyte molecule was monitored using UV-vis absorption spectroscopy (JASCO V-730), where the transmittance was measured after dropping and drying 2 μL of 100 μM R6G or CV ethanol solution onto the carbonized PAN nanomesh or a quartz glass plate (1 cm × 1 cm). Ethanol was used as a solvent instead of water to expedite the drying process. Density functional theory (DFT) calculations were performed using the Gaussian16 package.

2.3. SERS measurement

Samples were prepared by drop-casting an aliquot (2 μL) of an aqueous solution of CV or R6G onto a PAN-based substrate carbonized within the range of 240–1200 °C. The drops were allowed to dry at room temperature before measurement. SERS measurements were conducted using an RM2000 confocal Raman microscope (InVia, Renishaw PLC, England) with excitation at 532 and 633 nm through a 50× objective lens with a long working distance (NA 0.55). The SERS intensity was normalized *via* min–max normalization by dividing each intensity value by the difference between the maximum and minimum values of the spectra.

3. Results and discussion

3.1. Fabrication of PAN-based SERS substrates

Carbon-based SERS substrates were produced by carbonizing electrospun PAN nanomesh on Si wafers (Fig. 1(a)). First, PAN (M_W ~150 000) was dissolved in DMSO at a concentration of 8% wt/wt. The solution was stirred (400 rpm) for 6 h at 90 °C using a magnetic stirrer, resulting in a yellow, viscous solution. The PAN nanomesh was then prepared through electrospinning (NEX-101) at an applied voltage of 20 kV and a flow rate of 1 mL h^{-1}. The electrospun PAN nanomesh was easily manipulated and cut into desired shapes using scissors. It was then affixed to a Si wafer by spin coating (5 s at 500 rpm, followed by 30 s at 2700 rpm) the wafer with the PAN solution in DMSO (100 μL, 6% wt/wt) and then attaching the nanomesh. Si was chosen because of its high heat resistance, which was necessary in the subsequent steps. Subsequently, the PAN nanomesh was flameproofed in a furnace (CARBOLITE GELO 1200) for 2 h at 240 °C under release conditions, with a heating rate of 10 °C min^{-1}. After flameproofing, the PAN nanomesh, characterized by a black hue, was carbonized for 2 min in an evacuated furnace (FT-02VAC-50) at a temperature ranging from 600 °C to 1200 °C and a reduced pressure of 0.2 Pa. In the rest of this paper, the term ''carbonization'' refers to the initial flameproofing and subsequent steps at higher

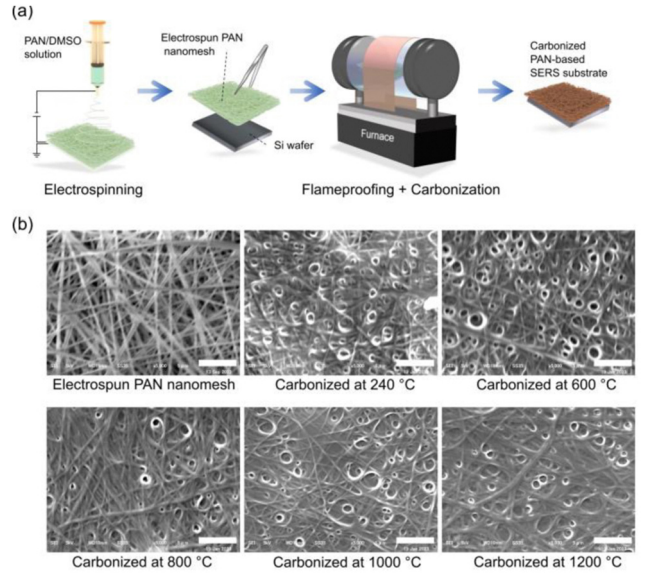

Fig. 1 PAN-based SERS substrates. (a) Fabrication process. This process starts with fabricating PAN nanomesh *via* electrospinning, which is attached to a silicon wafer to provide mechanical stability. The nanomesh is then flameproofed and carbonized to obtain the final SERS substrate. (b) SEM images of the electrospun PAN nanomesh and PAN-based SERS substrates flameproofed and then carbonized at 240–1200 °C. The sample treated at 240 °C underwent only the flameproofing step. Scale bars: 5 μm.

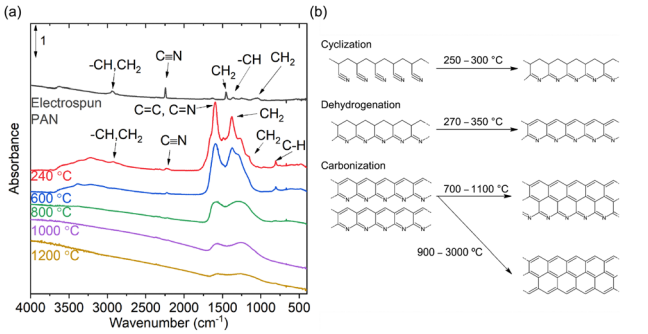

Fig. 2 Conjugated systems in the PAN-based SERS substrates. (a) IR spectra of the electrospun PAN nanomesh and PAN-based SERS substrates carbonized at 240–1200 °C. Spectra were shifted for ease of viewing. (b) Reactions occurring during the pyrolysis of PAN-based SERS substrates lead to the formation of a conjugated system.[31,39] The expansion of the conjugated system and formation of pyridinic N at the edges of the material can be observed at high temperatures.

temperatures. Samples carbonized at 240 °C are those subjected solely to the initial flameproofing step.

3.2. Characterization of PAN-based SERS substrates

Images of the PAN-based substrates were collected by SEM to investigate the morphological structure of the PAN substrates carbonized at various temperatures (Fig. 1(b)). Following flameproofing, a notable change in the surface morphology of the PAN-based substrate was obvious post-flameproofing, marked by the fusion and adherence of fibers, in contrast to the pre-flameproofing stage where fibers were apparent and dispersed. The presence of pores on the surface of the carbonized substrate resulted from the evaporation of DMSO within the fibers during the flameproofing stage. This led to a morphology that showed minimal variations across different carbonization temperatures. The presence of DMSO during the spin coating step was crucial for obtaining the desired fused fiber morphology. Without DMSO, the PAN fibers cannot fuse together, even at high temperatures (Fig. S1, ESI†). The fused fiber morphology played a crucial role in achieving significant SERS enhancements by decreasing the wettability of the resulting substrate (Fig. S2, ESI†). The limitation of aqueous sample diffusion within the substrate reduced the dispersion of the analyte and enhanced the effectiveness of Raman measurements. The fiber diameter remained approximately 0.3 μm before and after carbonization at temperatures below 800 °C, as analyzed using Digimizer image analysis software. However, at temperatures above 1000 °C, the diameter decreased to 0.1 μm (Fig. S3, ESI†).

IR spectroscopy was used to investigate the degree of carbonization of the PAN-based substrates treated at various temperatures by monitoring the peaks of the functional groups at the edges of the carbon chain (Fig. 2). The IR spectra peaks of the PAN-based substrates were assigned as follows: the peak associated with the C≡N group at 2220 cm^{-1} was barely detectable, even in the substrate carbonized at 240 °C,[44] indicating considerable reactivity of the C≡N groups in PAN after flameproofing. Following flameproofing, the PAN nanofibers exhibited a copper hue, indicating the presence of a C=N–C=N system.[45] Subsequently, the color darkened, probably due to the formation of a ladder structure.[46] Notably, the peak at 1590 cm^{-1}, not attributed to C=O because of the absence of prominent peaks in the 1650–1800 cm^{-1} range,[44] but to the stretching vibrations of C=C and C=N,[47] gradually shifted to a lower wavenumber with increasing carbonization temperature. This shift can be attributed to a decrease in C=N and an increase in C=C. Furthermore, the peak at 1590 cm^{-1} became broader and weaker, indicating an increase in the conjugated structure. Interestingly, as the carbonization temperature increased, the baseline increased at higher wavenumbers, indicating an increase in substrate scattering rather than absorption. Based on whether the IR peaks of the PAN functional groups were visible or not, the substrates were classified into two groups: those carbonized at 240–600 °C and those at 800–1200 °C. Specifically, the presence of the peak at 292 cm^{-1}, which denotes antisymmetric CH_2 stretching,[44] was evident in the IR spectra of the substrates carbonized at 240–600 °C, but absent in those at 800–1200 °C.[42] The presence of CH_2-related peaks implies incomplete dehydrogenation and condensation of cyclic structures in the substrates carbonized at 240–600 °C. In the substrate carbonized at 800 °C, peaks at 800 and 1370 cm^{-1}, which are related to the out-of-plane bending of C–H[47] and in-plane bending of C–H,[44,48] respectively, were observed. The presence of these peaks indicates limited intermolecular reactions that release hydrogen. Conversely, the IR spectra of substrates carbonized at 1000 °C and 1200 °C did not demonstrate peaks corresponding to the functional groups at the edge of the carbon chain, suggesting the formation of an extended

conjugated system with carbon atoms being exclusively bound to either C or N. Therefore, the carbonization process is considered to unfold in three distinct stages (Fig. 2(b)): (1) PAN chain cyclization and aromatic structure formation at ~250 °C; (2) cyclic structure dehydrogenation at 270–350 °C; and (3) N loss at 700–1100 °C (as also confirmed by EDS in Fig. S4, ESI†). These stages result in the condensation of unidimensional chains and the development of graphite-like domains, where N atoms are only present at the edges of the material. These terminal N atoms are referred to as "pyridinic N." The spontaneous Raman spectra further exhibit signs of carbonization progression at elevated temperatures (Fig. S5, ESI†). The intensity ratios of the D-band, mainly originating from the edge of the carbon chain,[49] to the G-band (*R*-values) decrease with increasing carbonization temperature.[50] Thus, the PAN-based substrate carbonized at 240–600 °C consisted of a one-dimensional polymer, while at temperatures of 800–1200 °C, an expanded conjugated system was present. These findings on the chemical changes in PAN during carbonization align with other reports published in the literature.[43,51]

To investigate the extent of N doping and evaluate the arrangement of chemical bonds, we performed XPS measurements (Fig. 3(a) and (b)). The peaks in the XPS spectra are presented in Table S1 (ESI†).[52] The elongated tails on the higher energy side of the C 1s and N 1s peaks indicated the presence of conjugated unsaturated bonds within the polymer.[53] These tails increased with increasing carbonization temperature, indicating an expansion of the conjugated system. Notably, the XPS results confirmed the same substrate groups as those identified by IR spectroscopy. The difference between the substrates carbonized at 240–600 °C and those carbonized at 800–1200 °C lies in the presence of a peak at 284 eV in the O 1s spectrum, which is attributed to carboxyl groups,[53] observed only in the spectra of the substrates carbonized at 240–600 °C. The carboxyl groups were produced as byproducts of cyclization reactions (Fig. S6, ESI†)[51] and disappeared from the surfaces of the PAN-based substrates carbonized at above 800 °C, resulting in a predominantly carbon-based material. These conclusions are supported by the notable agreement between the weight ratio information obtained using the XPS and EDS results (Fig. S4, ESI†). Finally, the appearance of graphitic N in the N 1s peak in the case of PAN-based substrates carbonized at >1000 °C is evident (Fig. 3(a) and (b)). The formation of graphitic N in the pyrolysis of PAN (Fig. 3(c)) has not been previously reported. The carbon atoms adjacent to graphitic N exhibit a significantly high positive charge density to counterbalance the strong electron affinity.[54] These are potentially important contributors to the SERS effect.

3.3. SERS performance

To evaluate the SERS performance of the PAN-based SERS substrates carbonized at different temperatures, we performed SERS measurements of R6G and CV by excitation at 532 and 633 nm (Fig. 4(a) and (b)). The baselines of the SERS spectra were corrected as described in the Methods section to enhance the clarity of the obtained spectra. Interestingly, the SERS

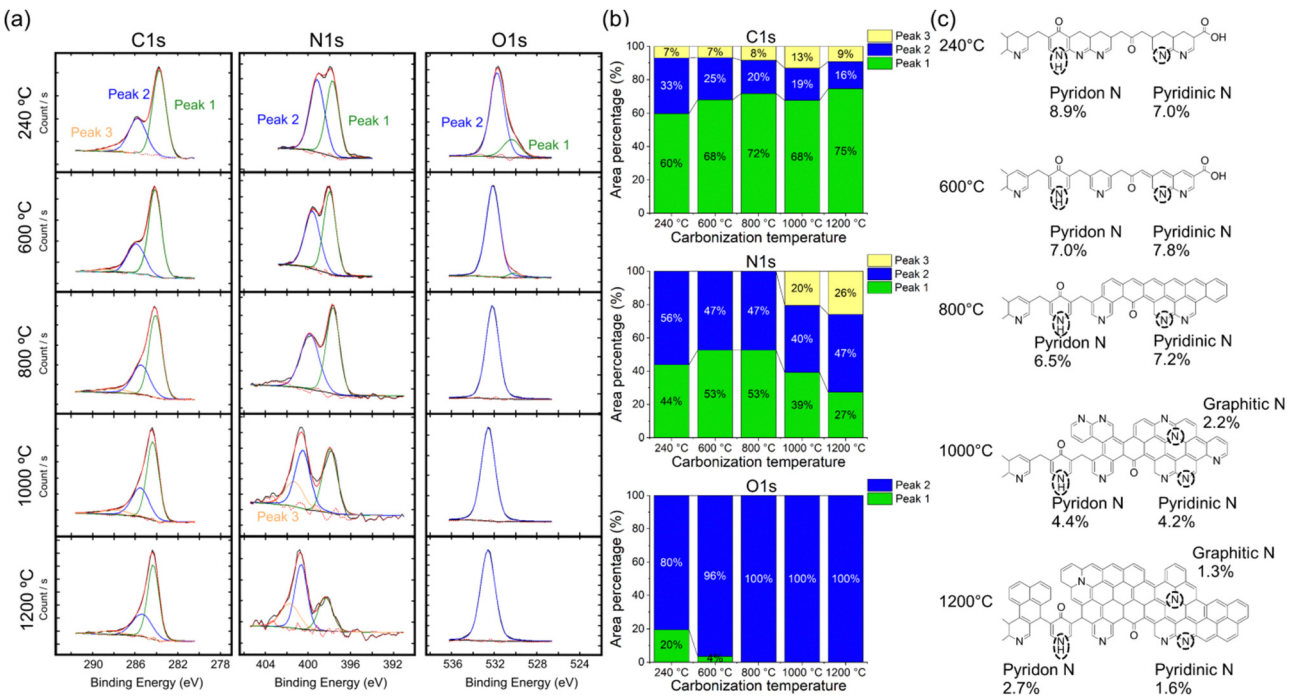

Fig. 3 Chemical structure of the PAN-based SERS substrates. (a) XPS spectra of the PAN-based SERS substrates carbonized at 240–1200 °C. Green, blue, and yellow curves correspond to peaks 1, 2, and 3, respectively. Peaks were fitted with the parameters given in Table S1 (ESI†). (b) Stacked columns of the peak areas in the XPS spectra. (c) Expected chemical structures of the PAN-based SERS substrates carbonized at 240–1200 °C calculated from the XPS N 1s peaks. The introduction of graphitic N as defects in the conjugated system can be observed at high temperatures.

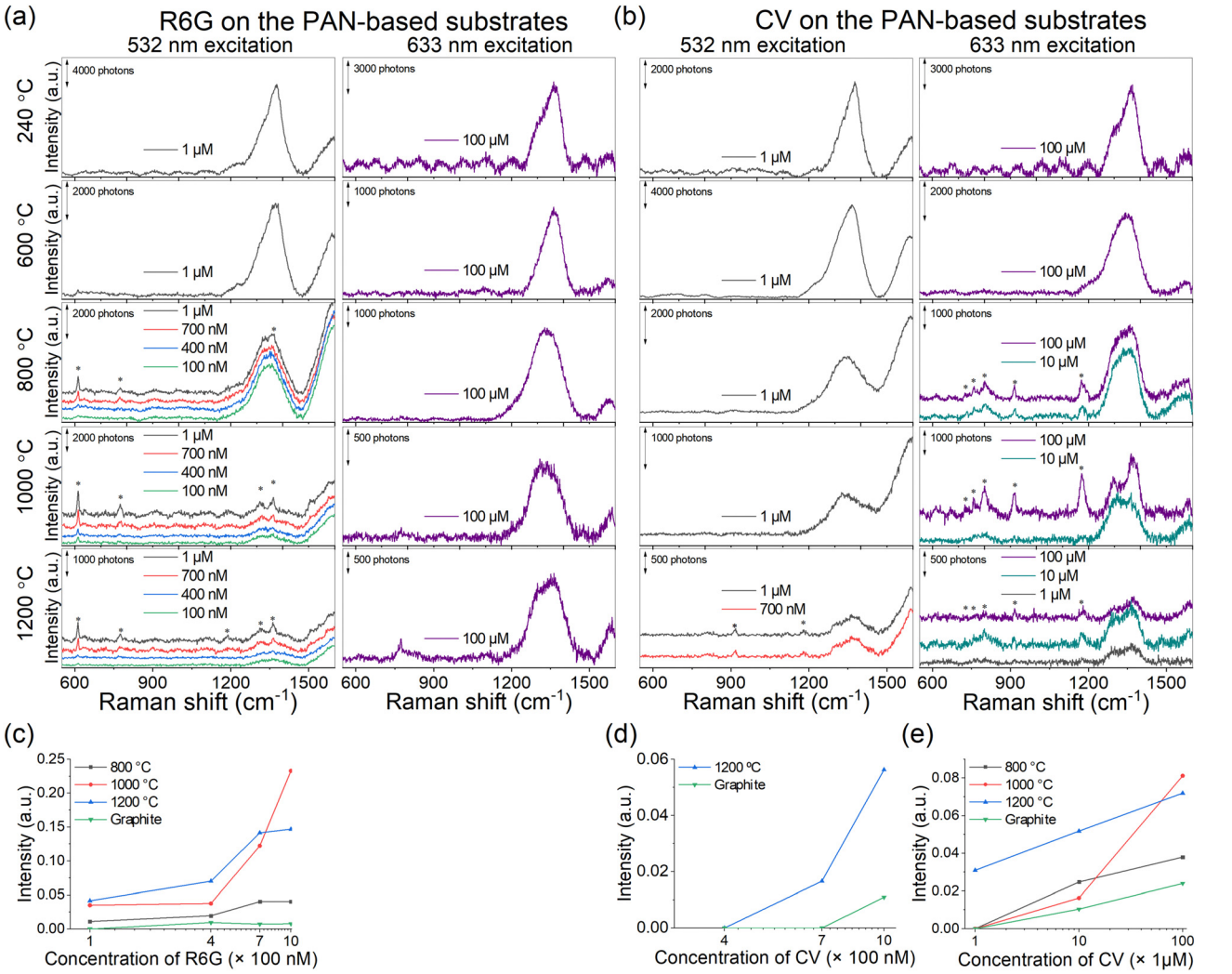

Fig. 4 SERS using PAN-based SERS substrates. Raman spectra of (a) R6G and (b) CV on the PAN-based SERS substrates carbonized at 240–1200 °C with 532 nm excitation (excitation power: 0.6 mW; exposure times: 10 s for the PAN-based substrate carbonized at 240 °C and 100 s for the PAN-based substrate carbonized at 600–1200 °C) and 633 nm excitation (excitation power: 1.2 mW for the PAN-based substrate carbonized at 240 °C and 600–1000 °C and 5.4 mW for the PAN-based substrate carbonized at 1200 °C; exposure times: 10 s for the PAN-based substrate carbonized at 240 °C and 100 s for the PAN-based substrate carbonized at 600–1200 °C) after baseline subtraction. Raman peaks of R6G are marked with asterisks (*). Normalized SERS peak intensities at different concentrations corresponding to (c) R6G's peak at 611 cm^{-1} with 532 nm excitation, (d) CV's peak at 916 cm^{-1} with 532 nm excitation, and (e) CV's peak at 916 cm^{-1} with 633 nm excitation. SERS intensities were normalized to the background intensity.

measurements were classified once again into the same groups identified by IR and XPS spectroscopy. Specifically, discernible Raman signals were obtained exclusively for the PAN-based substrates carbonized at 800–1200 °C. Despite the absence of morphological differences among PAN-based substrates carbonized at different temperatures (Fig. 1(b)), the SERS effect in substrates carbonized at 800–1200 °C surpasses the SERS effect's dependence on large surface areas. Fig. 4(c)–(e) illustrates the enhancement in the SERS intensities of samples with increasing carbonization temperature. The PAN-based substrates doped with N atoms demonstrated SERS EFs of 6800 and 3200 for R6G and CV, respectively. These values are approximately 30 times higher than those achieved using conventional graphite SERS substrates (Table S3, ESI†) and are comparable to those obtained using other N-doped carbon SERS substrates (Table S4, ESI†). The expansion of the conjugated system and more concentrated distribution of electronic orbitals in substrates carbonized at higher temperatures were likely to be attributed to this enhanced SERS effect. Particularly, the PAN-based substrate carbonized at 1200 °C for 2 min exhibited stronger SERS intensities than the graphite substrate, which is known for its expanded conjugated system. This observation can be attributed to the presence of surface heteroatomic dopants, such as graphitic N, which disrupt the π-conjugation and generate surface dipole moments. These chemical groups, characterized by polar structures, induce dipole–dipole interactions between the substrate and R6G or CV.[17] Therefore, a balance between the expansion of the conjugated system and the inclusion of graphitic N in substrates may contribute considerably to observing strong SERS effect.

3.4. Chemical enhancement mechanism

In the chemical-driven SERS process, enhancement in Raman signals is attributed to bidirectional CT originating from the highest occupied molecular orbital (HOMO) of the probe molecule to the conduction band of the SERS substrate and *vice versa*, *i.e.*, from the valence band of the SERS substrate to the lowest unoccupied molecular orbital (LUMO) of the probe molecule.[55] Within this CT framework, the density of states (DOS) function plays a crucial role in the SERS performance. The DOS within the conjugated configuration of the carbonized PAN, resembling a turbostratic graphite-like arrangement (as confirmed by XRD in Fig. S7, ESI†),[56] is remarkably concentrated within its conduction band.[57] This concentration facilitates a more efficient CT between the probe molecule and SERS substrate, thereby promoting enhanced SERS performance. However, as previously mentioned, SERS intensities for R6G and CV on the PAN-based substrate carbonized at 1200 °C surpassed those on a graphite substrate, and this remarkable enhancement can be attributed to the presence of graphitic N in the substrate.

To elucidate this increased efficiency, we examined the efficiency of CT between R6G and a PAN-based SERS substrate using DFT to calculate changes in the energy gap between the HOMO and LUMO states of R6G on carbonized PAN-based substrates. Fig. 5 shows the electron–hole distribution during the excitation process from the ground state to the first excited state of the complex between R6G and conjugated systems with pyridinic-N dopants, without N dopants, and with a graphitic-N dopant. For R6G on a conjugated system with pyridinic-N dopants, the excitation from S_0 to S_{12} is a local excitation in which both electrons and holes distribute on the conjugated system, namely, the whole excitation occurred on the conjugated system and resulted in a charge redistribution on the conjugated system without any effects on R6G molecule.

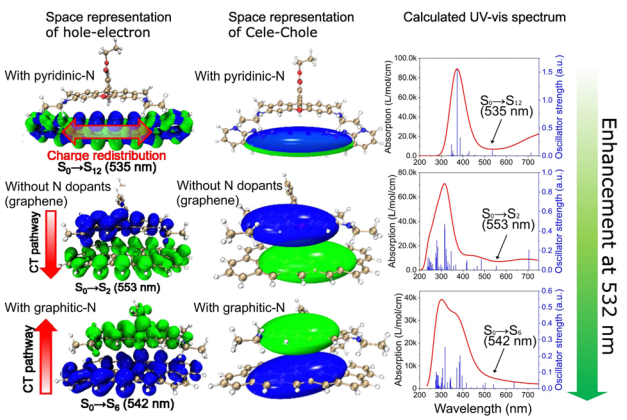

Fig. 5 Theoretical verifications for the chemical enhancement observed on the PAN-based SERS substrates. Electron–hole distribution (left), cele-chole distribution (middle), and calculated UV-vis spectra (right) of the complexes between R6G and conjugated systems with pyridinic-N dopants, without N dopants, and with a graphitic-N dopant from the ground state to the excited state during the electron excitation process obtained by time-dependent density functional theory (TDDFT) calculation with Gaussian16.

In contrast, for R6G on a conjugated system with a graphitic-N dopant or without N dopants, the holes mainly distribute on the conjugated system or R6G molecule, while the excited electrons distribute on the R6G molecule or the conjugated system, indicating that the excitation from S_0 to S_2 or S_6 of the complex is a CT excitation in which the charges are transferred from the conjugated system to R6G or from R6G to the conjugated system, respectively. The calculated UV-vis spectrum of the complex on the conjugated system with a graphitic-N dopant shows that the energy gap for the CT excitation (542 nm) is closer to 532 nm than that of the conjugated system without N dopants system (553 nm), which will generate a stronger resonant SERS effect. Thus, it is expected that each functional group of N has a different SERS performance. To confirm the potential CT between analytes and PAN-based SERS substrates, we performed UV-vis absorption measurements. Fig. S8 (ESI†) shows the absorption bands of R6G chemisorbed on the PAN-based substrate carbonized at 1200 °C, which were slightly redshifted than the absorption bands of R6G on a quartz glass. These redshifts indicate the emergence of a new electronic state that can act as a resonant intermediate for Raman scattering, suggesting that the Fermi level of the PAN-based substrate carbonized at 1200 °C is positioned between the HOMO and LUMO of R6G thereby resulting in CT excitations.[58] Therefore, we concluded that in the N-doped substrate carbonized at 1200 °C, the presence of graphitic N leads to changes in its Fermi level and an increase in its bandgap energy. Consequently, the PAN-based substrate carbonized at 1200 °C becomes an excellent platform for SERS based on the chemical mechanism.

3.5. Durability

To demonstrate the durability of the carbonized PAN-based substrate, we compared the SERS spectra of R6G collected on the PAN-based substrate carbonized at 1200 °C and on noble metal nanomesh[59–61] after prolonged laser irradiation (0.6 mW for 100 s). Notably, the PAN-based substrate carbonized at 1200 °C retained detectable Raman signals compared to the silver (Ag) nanomesh, as shown in Fig. 6(a) and (b), respectively. Fig. 6(c) shows the ratio of the residual SERS intensity at 611 cm^{-1} to the initial measurement intensity. The Raman peak intensities and the background fluorescence exhibited a gradual decrease with the irradiation time on both the PAN-based substrate and the Ag nanomesh. However, even after 900 s of irradiation, approximately 20% of the Raman intensity remained in the PAN-based substrate carbonized at 1200 °C, whereas only approximately 6% of the intensity remained in the Ag nanomesh. Traditional metal-based SERS substrates are susceptible to photothermal conversion through SPR during laser irradiation in the visible range. Prolonged or intense laser irradiation can lead to the photodegradation of probe molecules on metal-based SERS substrates, hindering their practical utility for biomolecule detection. In contrast, carbon-based SERS substrates lack SPR in the visible light region, making them insensitive to photothermal conversion – a key advantage of carbon-based substrates compared to

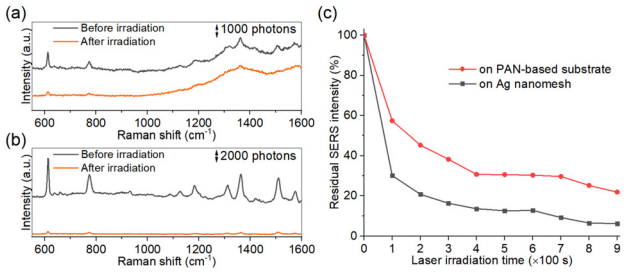

Fig. 6 Durability of the PAN-based SERS substrates. SERS spectra of R6G on (a) the PAN-based SERS substrate carbonized at 1200 °C and (b) Ag nanomesh before and after 900 s of irradiation. (c) Normalized SERS intensities corresponding to the peak at 611 cm^{-1} of R6G on the PAN-based SERS substrate carbonized at 1200 °C and Ag nanomesh obtained after different irradiation times.

metal ones. As a result, the durability against prolonged laser irradiation not only facilitates nondestructive SERS measurements of biomolecules but also enables continuous and real-time monitoring, including chemical reaction analysis and degradation tracking, which require longer irradiation time.

Conclusions

In this study, we developed a simple and controllable fabrication method for producing N-doped carbon-based SERS substrates with enhanced SERS efficiency. The carbonization process of the electrospun PAN nanomesh enabled us to control the expansion of the conjugated system and the presence of N dopants at functional levels by varying the carbonization temperature alone. Importantly, we demonstrated how PAN-based SERS substrates carbonized at 1000–1200 °C contained graphitic N, a structure that has not been previously proposed for PAN pyrolysis. The presence of graphitic N contributes to the enhancement of the SERS efficiencies *via* the chemical mechanism for R6G and CV, as demonstrated using DFT calculations. The SERS efficiency was not only higher than that of the PAN-based substrate carbonized at 800 °C, but also surpasses that of a standard graphite substrate without graphitic N. This optimal efficiency is attributed to the interplay between two competing reactions: the expansion of the conjugated system and the effect of N doping, reaching an optimal balance at a carbonization temperature of 1200 °C. Considering that the starting material, PAN nanomesh, possesses tunable shape and mechanical properties and that the resulting SERS substrates exhibit remarkable durability against prolonged laser irradiation in the visible range, the PAN-based SERS substrates are an excellent choice for various sensing applications across diverse devices.

Author contributions

M. M. performed the experiments and analyzed the experimental data. X. T. conducted the DFT calculations. M. M., F. L., Y. K., and K. G. wrote the paper. All authors reviewed the paper. Y. K., T.-H. X., and K. G. supervised the work. K. G. acquired the funding to support the work.

Conflicts of interest

K. G. is a shareholder of LucasLand.

Acknowledgements

This study was mainly supported by MEXT Quantum Leap Flagship Program (JPMXS0120330644), JSPS KAKENHI (JP20K 14785), Murata Science Foundation, JSPS Core-to-Core Program (JPJSCCA20190007), JSPS Bilateral Program (JPJSBP120227703), White Rock Foundation, University of Tokyo GAP Fund, UTokyo IPC, Mohammed bin Salman Center for Future Science and Technology for Saudi-Japan Vision 2030 at the University of Tokyo, MEXT Advanced Research Infrastructure for Materials and Nanotechnology in Japan (ARIM) (22UT0168, 23UT1083), and JST SPRING (JPMJSP2108). P. K. D acknowledges Indo-Japan bilateral funding (DST/INT/JSPS/P-352/2022).

Notes and references

1 B. Sharma, R. R. Frontiera, A.-I. Henry, E. Ringe and R. P. Van Duyne, *Matter. Today*, 2012, **15**, 16–25.
2 X. X. Han, R. S. Rodriguez, C. L. Haynes, Y. Ozaki and B. Zhao, *Nat. Rev. Methods Primers*, 2021, **1**, 87.
3 A. Campion and P. Kambhampati, *Chem. Soc. Rev.*, 1998, **27**, 241.
4 T. Itoh, M. Procházka, Z. C. Dong, W. Ji, Y. S. Yamamoto, Y. Zhang and Y. Ozaki, *Chem. Rev.*, 2023, **123**, 1552–1634.
5 P. L. Stiles, J. A. Dieringer, N. C. Shah and R. P. Van Duyne, *Annu. Rev. Anal. Chem.*, 2008, **1**, 601–626.
6 S. Bai, X. Ren, K. Obata, Y. Ito and K. Sugioka, *Opto-Electron. Adv.*, 2022, **5**, 210121.
7 Z. Pei, J. Li, C. Ji, J. Tan, Z. Shao, X. Zhao, Z. Li, B. Man, J. Yu and C. Zhang, *J. Phys. Chem. Lett.*, 2023, **14**, 5932–5939.
8 N. V. Mazur, O. A. Kapush, O. F. Isaieva, S. I. Budzulyak, A. Yu. Buziashvili, Y. V. Pirko, M. A. Skoryk, A. I. Yemets, O. M. Hreshchuk, V. O. Yukhymchuk and V. M. Dzhagan, *Phys. Chem. Solid State*, 2023, **24**, 682–691.
9 X. Luo, R. Pan, M. Cai, W. Liu, C. Chen, G. Jiang, X. Hu, H. Zhang and M. Zhong, *Sens. Actuators, B*, 2021, **326**, 128826.
10 V. Dzhagan, N. Mazur, O. Kapush, M. Skoryk, Y. Pirko, A. Yemets, V. Dzhahan, P. Shepeliavyi, M. Valakh and V. Yukhymchuk, *ACS Omega*, 2024, **9**, 4819–4830.
11 M. L. Coluccio, G. Das, F. Mecarini, F. Gentile, A. Pujia, L. Bava, R. Tallerico, P. Candeloro, C. Liberale, F. De Angelis and E. Di Fabrizio, *Microelectron. Eng.*, 2009, **86**, 1085–1088.
12 A. Virga, P. Rivolo, F. Frascella, A. Angelini, E. Descrovi, F. Geobaldo and F. Giorgis, *J. Phys. Chem. C*, 2013, **117**, 20139–20145.
13 J. Yu, J. Wu, H. Yang, P. Li, J. Liu, M. Wang, J. Pang, C. Li, C. Yang and K. Xu, *ACS Appl. Mater. Interfaces*, 2022, **14**, 43877–43885.
14 S. Jin, D. Zhang, B. Yang, S. Guo, L. Chen and Y. M. Jung, *Analyst*, 2024, **149**, 11–28.

15 Y. Hu, Á. I. López-Lorente and B. Mizaikoff, *ACS Photonics*, 2019, **6**, 2182–2197.
16 H. Lai, F. Xu, Y. Zhang and L. Wang, *J. Mater. Chem. B*, 2018, **6**, 4008–4028.
17 P. M. Pancorbo, H. Zhang, X. Yu, T. H. Xiao and K. Goda, *Europhys. Lett.*, 2021, **136**, 34001.
18 D. Qi, L. Lu, L. Wang and J. Zhang, *J. Am. Chem. Soc.*, 2014, **136**, 9886–9889.
19 Z. Zheng, S. Cong, W. Gong, J. Xuan, G. Li, W. Lu, F. Geng and Z. Zhao, *Nat. Commun.*, 2017, **8**, 1993.
20 S. Cong, Z. Wang, W. Gong, Z. Chen, W. Lu, J. R. Lombardi and Z. Zhao, *Nat. Commun.*, 2019, **10**, 678.
21 M. Yilmaz, E. Babur, M. Ozdemir, R. L. Gieseking, Y. Dede, U. Tamer, G. C. Schatz, A. Facchetti, H. Usta and G. Demirel, *Nat. Mater.*, 2017, **16**, 918–924.
22 N. Chen, T. H. Xiao, Z. Luo, Y. Kitahama, K. Hiramatsu, N. Kishimoto, T. Itoh, Z. Cheng and K. Goda, *Nat. Commun.*, 2020, **11**, 4772.
23 X. Ling, L. Xie, Y. Fang, H. Xu, H. Zhang, J. Kong, M. S. Dresselhaus, J. Zhang and Z. Liu, *Nano Lett.*, 2010, **10**, 553–561.
24 Y.-S. Sun, C. F. Lin, S. T. Luo and C. Y. Su, *ACS Appl. Mater. Interfaces*, 2017, **9**, 31235–31244.
25 D. Liu, X. Chen, Y. Hu, T. Sun, Z. Song, Y. Zheng, Y. Cao, Z. Cai, M. Cao, L. Peng, Y. Huang, L. Du, W. Yang, G. Chen, D. Wei, A. T. S. Wee and D. Wei, *Nat. Commun.*, 2018, **9**, 193.
26 L. Ji, G. Guo, H. Sheng, S. Qin, B. Wang, D. Han, T. Li, D. Yang and A. Dong, *Chem. Mater.*, 2016, **28**, 3823–3830.
27 L. Zhang, M. Yin, J. Li, G. Wei, H. Bai, G. Xi and L. Mao, *Anal. Chem.*, 2022, **94**, 13659.
28 A. Silver, H. Kitadai, H. Liu, T. Granzier-Nakajima, M. Terrones, X. Ling and S. Huang, *Nanomaterials*, 2019, **9**, 516.
29 L. Yang, J. Hu, L. He, J. Tang, Y. Zhou, J. Li and K. Ding, *Chem. Eng. J.*, 2017, **327**, 694–704.
30 S. H. Gaikwad and S. P. Mukherjee, *ACS Appl. Nano Mater.*, 2021, **4**, 11611–11624.
31 M. Keshavarz, A. K. M. R. H. Chowdhury, P. Kassanos, B. Tan and K. Venkatakrishnan, *Sens. Actuators, B*, 2020, **323**, 128703.
32 Y.-S. Sun, C.-F. Lin and S.-T. Luo, *J. Phys. Chem. C*, 2017, **121**, 14795–14802.
33 C.-Y. Chang, Y.-S. Sun, Y.-W. Yang, C.-H. Wang, S.-L. Cheng and W.-W. Hu, *ACS Appl. Nano Mater.*, 2020, **3**, 858–868.
34 J. Lin, D. Zhang, J. Yu, T. Pan, X. Wu, T. Chen, C. Gao, C. Chen, X. Wang and A. Wu, *Anal. Chem.*, 2023, **95**, 4671–4681.
35 X. Tang, N. Kishimoto, Y. Kitahama, T.-T. You, M. Adachi, Y. Shigeta, S. Tanaka, T.-H. Xiao and K. Goda, *J. Phys. Chem. Lett.*, 2023, **14**, 10208–10218.
36 K. Tantiwanichapan, X. Wang, H. Durmaz, Y. Li, A. K. Swan and R. Paiella, *ACS Photonics*, 2017, **4**, 2011–2017.
37 P. Rani and V. K. Jindal, *RSC Adv.*, 2013, **3**, 802–812.
38 M. Shao, C. Ji, J. Tan, B. Du, X. Zhao, J. Yu, B. Man, K. Xu, C. Zhang and Z. Li, *Opto-Electron. Adv.*, 2023, **6**, 230094.
39 S. Ren, L. Dong, X. Zhang, T. Lei, F. Ehrenhauser, K. Song, M. Li, X. Sun and Q. Wu, *Materials*, 2017, **10**, 68.
40 N. Hedin, V. Sobolev, L. Zhang, Z. Zhu and H. Fong, *J. Mater. Sci.*, 2011, **46**, 6453–6456.
41 Y. Wang, Q. Yang, G. Shan, C. Wang, J. Du, S. Wang, Y. Li, X. Chen, X. Jing and Y. Wei, *Mater. Lett.*, 2005, **59**, 3046–3049.
42 L. Zhang, A. Aboagye, A. Kelkar, C. Lai and H. Fong, *J. Mater. Sci.*, 2014, **49**, 463–480.
43 R. Janus, P. Natkański, A. Wach, M. Drozdek, Z. Piwowarska, P. Cool and P. Kuśtrowski, *J. Therm. Anal. Calorim.*, 2012, **110**, 119–125.
44 R. B. Mathur, D. Gupta, O. P. Bahl and T. L. Dhami, *Fibre Sci. Technol.*, 1984, **20**, 227–234.
45 W. Watt and W. Johnson, *Nature*, 1975, **257**, 210–212.
46 M. S. A. Rahaman, A. F. Ismail and A. Mustafa, *Polym. Degrad. Stab.*, 2007, **92**, 1421–1432.
47 T. Sun, Y. Hou and H. Wang, *J. Appl. Polym. Sci.*, 2010, **118**, 462–468.
48 H. Kakida and K. Tashiro, *Polym. J.*, 1997, **29**, 353–357.
49 T. W. Hu, D. Y. Ma, F. Ma and K. W. Xu, *Appl. Phys. Lett.*, 2012, **101**, 241903.
50 C. Kim, S. H. Park, J. I. Cho, D. Y. Lee, T. J. Park, W. J. Lee and K. S. Yang, *J. Raman Spectrosc.*, 2004, **35**, 928–933.
51 K. Nukada and K. Kobori, *Kobunshi*, 1974, **23**, 445–448.
52 P. Lazar, R. Mach and M. Otyepka, *J. Phys. Chem. C*, 2019, **123**, 10695–10702.
53 T. Takahagi, I. Shimada, M. Fukuhara, K. Morita and A. Ishitani, *J. Polym. Sci. A*, 1986, **24**, 3101–3107.
54 K. Gong, F. Du, X. Zhenhai, M. Durstock and L. Dai, *Science*, 2009, **323**, 760–764.
55 J. R. Lombardi, R. L. Birke, T. Lu and J. Xu, *J. Chem. Phys.*, 1986, **84**, 4174–4180.
56 S. M. Saufi and A. F. Ismail, *Carbon*, 2004, **42**, 241–259.
57 S. S. Zade, N. Zamoshchik and M. Bendikov, *Acc. Chem. Res.*, 2011, **44**, 14–24.
58 L. Xia, M. Chen, X. Zhao, Z. Zhang, J. Xia, H. Xu and M. Sun, *J. Raman Spectrosc.*, 2014, **45**, 533–540.
59 V. Kesava Rao, X. Tang, Y. Sekine, M. Egawa, P. K. Dwivedi, Y. Kitahama, W. Yang and K. Goda, *Adv. Photonics Res.*, 2024, **5**, 2300291.
60 Y. Kitahama, P. M. Pancorbo, H. Segawa, M. Marumi, T.-H. Xiao, K. Hiramatsu, W. Yang and K. Goda, *Anal. Methods*, 2023, **15**, 1028–1036.
61 L. Liu, P. M. Pancorbo, T.-H. Xiao, S. Noguchi, M. Marumi, H. Segawa, S. Karhadkar, J. Gala de Pablo, K. Hiramatsu, Y. Kitahama, T. Itoh, J. Qu, K. Takei and K. Goda, *Adv. Opt. Mater.*, 2022, **10**, 2200054.